The uncanny weight of granular columns

Author: Iker Zamorano Vega
Advisor: Ramon Planet, Alberto Fernández-Nieves
Facultat de Física, Universitat de Barcelona, Diagonal 645, 08028 Barcelona, Spain.

Abstract: The results obtained by Janssen in 1895 showed that when filling a silo with corn, there is a certain point where the pressure measured at the bottom saturates and does not linearly increase with added mass. Recent work with spherical grains found that when the silo is narrow enough a reverse Janssen effect is found and the pressure, rather than just saturate first increases faster than linearly due to the configuration the grains adopt inside the container. Via experimental investigation this work demonstrates that this behaviour is still fulfilled when changing the geometry of the grain to an oblate ellipsoid and that the deviation from fluid behaviour requires less added mass due to the larger packing fraction acquired in this case.

I. INTRODUCTION

It was 1895 when the German engineer H.A. Janssen performed experiments with granular particles aimed at designing strong silos to maintain the grain [1,2]. To do so, he measured the pressure exerted by the grains at the bottom of the container as a function of the added mass, as shown in Fig.(1).

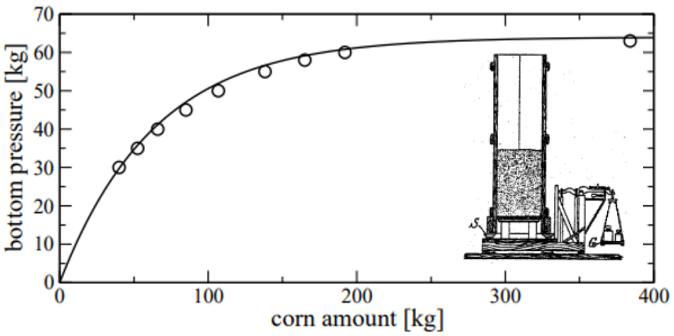

FIG. 1: Janssen's original results of the pressure (in kg) at the bottom of a silo versus the amount of corn added (also in kg). The inset is the original sketch of the Janssen's original experimental setup. The data and the sketch have been extracted from [2].

Let us first discuss the case of filling a container with water. In this case, as we know from experience, the more liquid we add, the more it weights and the larger the pressure P it exerts at the bottom. In fact, in this case:

$$P(z) = \rho g z \,, \qquad (1)$$

where z represents the depth, ρ is the density of the fluid and g is the gravitational acceleration on Earth, taken as approximately $g = 9.81$ m/s^2.

In contrast to the case of water, Janssen found that, when filling a container with corn grains instead of with liquid, the pressure showed a saturation regime above certain added mass and consequently, above a given height. The force per unit area that the grains exert over the bottom of the container remains constant despite you continue add grains. As a result of this unexpected behaviour, this experimental result became a benchmark for further work involving granular media.

One of those posterior works [3] used modern techniques to determine the validity of the result obtained by Janssen back then. It reaffirmed the continuum model proposed by Janssen [1,2], finding the saturation of the pressure with added mass.

More recently, the group I am working on with revisited Janssen's work by using spherical plastic beads [4] with diameter $\sigma = (5.94 \pm 0.02)$ mm and mass $M = (112.6 \pm 0.1)$ mg, but using cylindrical containers that were narrower than the ones used by Janssen. Their diameters D were $D \leq 30\sigma$. A new regime was found in [4], the measured mass was higher than the added mass (a reversed Janssen effect), followed by the saturation regime typical of Janssen.

This discovery opens the door to additional work with, for example, other grain shapes. Amazed by the non-intuitive results in such a simple experiment, I decided to take the chance on working with the group. My work consists in doing similar experiments to those that were done in [4] but using grains with different geometry. Spherically oblate elipsoids will be used instead of spheres, in order to determine if the shape of the grain affects the behaviour.

II. PHENOMENOLOGICAL MODELIZATION

We can describe the observed behaviour using a physical model. Along this section I will discuss the model that Janssen used to describe his experiments [1,2], as well as the one developed for the behaviour seen in shallower containers [4].

A. The elastic sea with friction

Janssen's results can be rationalized by considering that what prevented the grains to raise the pressure at the bottom of the silo was the friction between the grains and the walls of the container, which he considered to be at the Coulomb's threshold. In [2], the equation that describes the pressure is derived considering the granular media as a continuum, commonly known as "elastic sea", and applying the condition of mechanical equilibrium to a cylindrical slice. This treatment for the grains comes with the consideration that the radial component of the stress is proportional to the vertical component by a proportionality constant k:

$$\sigma_{zz} = k\,\sigma_{rr} = k\,\sigma_{\varphi\varphi} \qquad (2)$$

$$P = -\sigma_{zz} \qquad (3)$$

Relations (2) and (3) between pressure and the components of the stress tensor implies that the surfaces of equal pressure for the elastic sea are horizontal in both the absence and presence of friction. With all this in mind, we can find the differential equation for the longitudinal component of the stress tensor, σ_{zz} , obtaining:

izamorve7@alumnes.ub.edu

$$\frac{d\sigma_{zz}}{dz} = -\rho g - \frac{2\,k\,\mu_s}{R}\,\sigma_{zz}\,. \qquad (4)$$

Where ρ is the density of the media, R is the radii of the circular cross section of the cylindrical container and μ_s is the friction coefficient at Coulomb's threshold. If we integrate Eq.(4) applying the bounding condition that $\sigma_{zz}(z=0) = 0$ and defining $\lambda \equiv \frac{R}{2\mu_s k}$ and using Eq.(3), we obtain:

$$P(z) = \rho g \lambda\,(1 - e^{\frac{-z}{\lambda}}) \qquad (5)$$

This expression is what Janssen obtained as the solution for his problem [1,2], all material details are embedded into λ. In Fig.(2) we plot the result and compare it with the pressure that a fluid would have. As we can see, Eq.(5) reproduces a similar behaviour to the experimental results shown in Fig.(1).

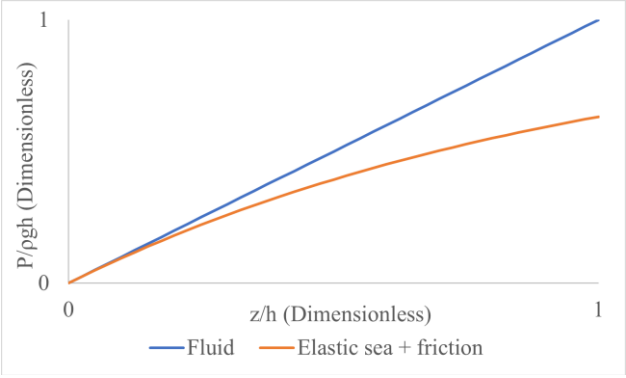

FIG. 2: Comparison between the normalized pressure of an ideal fluid and the normalized pressure obtained in Eq.(5) versus a normalized depth.

Despite the model qualitatively captures the experiments, we know that some assumptions do not hold in reality. For example, the model assumes horizontal isobar surfaces and, as discussed in [5], these surfaces can in reality be concave or convex. The curvature of the surfaces is directly related to the frictional forces acting between the media and the walls of the container. If the surface is concave (seen from below) the resultant forces act in the opposite sense to gravity and therefore, are the ones responsible for the saturation regime. Convex surfaces could also be expected and would imply that the frictional forces acted in the same sense as gravity, leading to higher effective masses measured at the bottom of the container. The latter, however, were not found until the experiments with cylinders of smaller diameters [4]. Due to the fact that Eq.(5) does not describe these compressive forces, a new model was required.

B. The overshoot model

The experiments realized in [4] consisted on adding spheres in chunks into the cylinder and letting them reach mechanical equilibrium before adding additional chunks of spheres. This was repeated adding the same plastic beads in cylindrical recipients with different diameters. The effect was also studied numerically, by using simulations in which spheres with mass M and diameter σ were added into cylinders with diameter D, and assuming Coulomb's threshold was fulfilled for both the wall-sphere contact and the sphere-sphere contacts. The main advantage of doing these simulations is that you can visualize the forces inside the cylinder and their distribution.

There are three characteristic heights found in these experiments that allows us to compare the measurements for different D. The first one is h_a, the height at which the system starts deviating from the fluid behaviour. The second one is h^*, the height at which one finds the maximum deviation of the apparent mass form the added mass. Lastly, we have h_d, which is the height at which the system crosses again the dependence of the fluid behaviour and enters into the saturation regime that Janssen originally found and described.

The results can be described by the following continuity equation for the pressure:

$$\frac{dP}{dz} = \rho g - \frac{4}{\sigma}\tau(z)\,, \qquad (6)$$

where $\tau(z)$ is the stress, which depends on frictional forces and the number of contacts per unit length:

$$\tau(z) = \frac{n_c(D)\langle F_w(z)\rangle}{\pi D}. \qquad (7)$$

Here $\langle F_w(z)\rangle$ is the average frictional force for each sphere at a considered depth z and $n_c(D)$ the number of contacts per unit length. The value of $\langle F_w(z)\rangle$ was taken as $\langle F_w(z)\rangle = 0$ for depths $z<h_a$, equal to $\langle F_w(z)\rangle = F_c$ for region $h_a<z<h^*$, where $F_c < 0$ is the frictional force at Coulomb's threshold. Finally, for region $z > h^*$:

$$\langle F_w(z)\rangle = k\pi D P(z)\left(1 - e^{\frac{-(z-h^*)}{\xi}}\right), \qquad (8)$$

where $\xi \approx 6\sigma$ is an experimentally found decay length. By solving Eq.(6) up to the regime where $z<h^*$, we find that

$$max\left[\frac{m_a}{m}\right] - 1 = \frac{F_c n_c(D)}{\pi\rho g D^2}\left(1 - \frac{h_a}{h^*}\right). \qquad (9)$$

Therefore, the model predicts that the maximum deviation from the fluid behaviour varies with D as $\sim 1/D$, since $n_c(D) \sim D$, as shown in the supplemental material of [4]. These expectations are on agreement with both experiments and simulation. Note that if we consider containers with large diameters, we recover Janssen's results [1,2], where the reverse Janssen effect is absent.

C. The packing fraction

Given that the continuity equation (6) has a dependence on the number of contacts $n_c(D)$, it is relevant to introduce the packing fraction. Which is defined as:

$$f = \frac{Occupied\ volume}{Available\ volume} \qquad (10)$$

The possible arrangements of the grains leads to different values of the packing fraction. This may change the number of contacts and impact the results for the measured apparent mass. Another important aspect, since I am going to work with ellipsoids instead of spheres, is that the occupied volume

depends on the geometry of the grain, since the number of contacts required for mechanical equilibrium depends on grain geometry.

There are several ways of distributing spheres, but we will focus on random close packing, which is a way of placing spheres inside a volume with no preferred disposition. The maximum packing expected for this case is about 64% [6,7]. Another value of interest is random packing of oblate ellipsoids, since it is the geometry I am going to work with here. From [8] we can see that the packing fraction of an ellipsoid with semiaxes *a*, *b* and *c*, depends on its aspect ratio $\alpha = a/b$. For α = 0.5 we would expect a random close packing fraction between 60% and 70%. In this case:

$$f_{ellipsoid} = \frac{N\,\frac{4}{3}\pi abc}{\pi R^2 h} = \frac{4N}{3}\left(\frac{abc}{R^2 h}\right) \qquad (11)$$

where *h* and *R* are the height of the granular column and radius of the cylindrical container, and *N* is the number of grains.

III. EXPERIMENTAL WORK

A. Set up and experimental procedure

The grains used for these experiments are lentils since they can be characterized as an oblate ellipsoid. They are relatively monodisperse, since their dimensions do not differ enormously from grain to grain. To determine the characteristic of the ones I have used along these experiments, I measured the mass of 30 lentils with an analytic scale with a sensitivity of δm= 0.1 mg. For axes, *a* and *b* we used a *MatLab* program to analyse an image from the grains, and determined *c* using a calliper whose sensitivity is δc= 0.05 mm over 30 grains. A characteristic mean diameter $\sigma = 2\sqrt[3]{abc}$ is also defined. The values of the parameters of the lentils are shown in Table I.

***a* (mm)**	2.58 ± 0.05	***M* (mg)**	35.950 ± 0.003
***b* (mm)**	2.40 ± 0.05	***V* (mm^3)**	31.6 ± 0.9
***c* (mm)**	1.23 ± 0.01	***P* (g/cm^3)**	1.14 ± 0.03
α	0.49 ± 0.01	**σ (mm)**	3.92 ± 0.01

TABLE I: Experimental values for a single lentil. We report the axes, aspect ratio, mass, volume, density, and characteristic diameter. The errors have been computed by considering the sensitivity of the instruments, the standard error of the mean and propagation errors.

We used, three cylinders with diameters measured with the caliper. The values of *D* and of D/σ are shown in Table II.

Cylinder	*D* (mm)	D/σ
Small	20.45 ± 0.05	5.21 ± 0.02
Medium	34.10 ± 0.05	8.69 ± 0.03
Large	49.15 ± 0.05	12.52 ± 0.05

TABLE II: Experimental values for the diameters and the characteristic ratios of the three different cylinders. The errors have been computed by considering the sensitivity of the instruments and error propagation.

We used the same analytic scale as for measuring the weight of the lentils, two cameras (one to capture the value that the scale indicates and the other to capture the cylinder with the lentils) and a support with a hook for sustaining the cylinder right above the analytic scale. The complete set us is shown in Fig.(3).

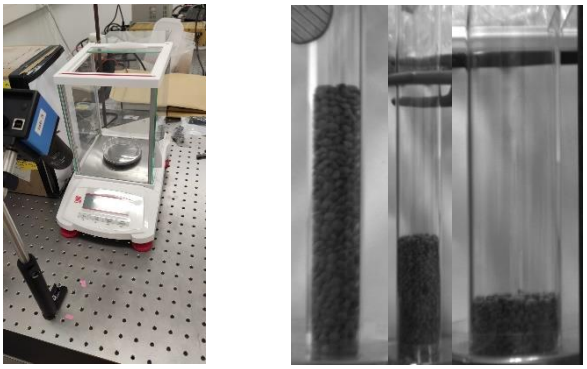

FIG.3: LEFT: Picture of the experimental set up. RIGHT: Images of lentils poured inside the three different cylindrical containers. From left to right *D* increases.

To begin the experiment, I put the cylinder on the analytic scale supported by a hook, so that it does not touch the scale itself, since the function of the container is just to form a granular column. Then I add 30 lentils inside the cylinder in small chunks and I wait five seconds before measuring. We do this to let the system reach mechanical equilibrium. It is not optimal to wait much longer, since the system seems to exhibit time dependence. Each measurement consists on taking one photo with each camera, and right after, I add another 30 lentils and repeat the process until I get the number of measurements desired. Then, the photos are analysed using *MatLab* to get the height and the effective mass of the lentils added at each step. The experiment is realised three times for each cylinder in order to get some statistics.

B. Experimental results

After data collection, we plot the apparent mass *ma* versus the added mass *m*. The following values are of special interest: m_a (added mass where the system deviates from fluid behaviour), m^* (added mass where the system reaches its maximum deviation from fluid behaviour) and m_d (added mass where the system enters into the saturation regime). The packing fraction will also be computed.

The results for the small, medium and large cylinders are shown in Figs.(4), (5) and (6) respectively. The corresponding values for m_a, m^* and m_d are shown in Tables III, IV and V.

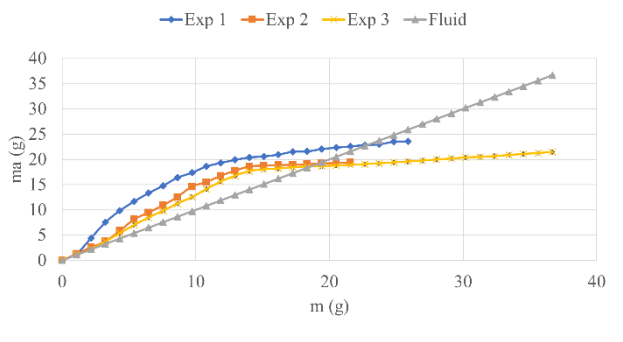

FIG.4: Representation of the experimental results for D/σ = 5.21**.** We see the effective mass *ma* versus the added mass *m* for the three experiments compared with the behaviour for a fluid in the small cylinder.

	m_a (g)	m^* (g)	m_d (g)	f (%)
#1	1.1 ± 0.2	11.86 ± 0.04	22.6 ± 1.0	-
#2	2.2 ± 0.4	11 ± 2	19.4 ± 0.7	-
#3	2.16 ± 0.04	14.0 ± 1.0	18.3 ± 1.2	-

TABLE III: Experimental results obtained for the cylinder with ratio D/σ = 5.21 *for* m_a, m^* *and* m_d and its packing fraction *f*.

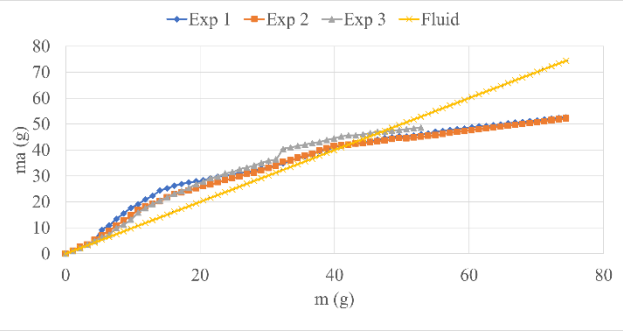

FIG.5: Representation of the experimental results for D/σ = 8.69**.** We see the effective mass *ma* versus the added mass *m* for the three experiments compared with the behaviour for a fluid in the medium cylinder.

	m_a (g)	m^* (g)	m_d (g)	f (%)
#1	3.24 ± 0.14	15.10 ±0.04	42.06 ± 0.14	65±3
#2	3.24 ± 0.09	17.24 ±0.04	42.06 ± 0.09	73.4±0.5
#3	3.24 ± 0.12	22.6 ± 1.1	47.5 ± 0.6	67.9±1.1

TABLE IV: Experimental results obtained for the cylinder with ratio D/σ = 8.69 *for* m_a, m^* *and* m_d and its packing fraction *f*.

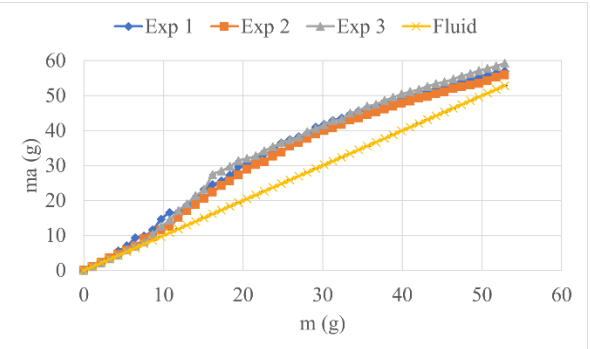

FIG.6: Representation of the experimental results for D/σ = 12.52**.** We see the effective mass *ma* versus the added mass *m* for the three experiments compared with the behaviour for a fluid in the larger cylinder.

	m_a (g)	m^* (g)	m_d (g)	f (%)
#1	3.24 ± 0.02	30.20 ± 0.04	-	74 ± 4
#2	6.5 ± 0.4	30.20 ± 0.04	-	70 ± 4
#3	7.5 ± 0.4	26 ± 2	-	73 ± 4

TABLE V: Experimental results obtained for the cylinder with ratio D/σ = 12.52 *for* m_a, m^* *and* m_d and its packing fraction *f*.

C. Discussion of results

As shown in Figs.(4)-(6), lentils seem to behave similar to spheres when placed in narrow cylinders. We can clearly identify the reverse and conventional Janssen effects. For the large cylinder though none of the experiments reaches the saturation regime, mainly because the amount of added mass was not enough to reach it. If we compare Fig.(5) with the experimental results for D/σ=8.2 in [4], the ellipsoids seem to reach the overshoot earlier. However, the maximum deviation from the fluid behaviour is similar in both cases, as well as the point where the systems enters the saturation regime.

As for the values of m_a, m^* and m_d, all of them seem to increase as the diameter of the container increases. This is because the system requires a certain height in order to form concave or convex surfaces with equal pressure, which are responsible for measuring less or more mass than the one that has been added to form. Note the value for m_d in the largest cylinder has not been determined because the system does not reach saturation. However, by extrapolation, we expect that m_d falls between 55 g and 60 g.

Because of the similarity of our results to those obtained for spheres, I compare what is expected from Eq.(9) to my results to see if the results for spheres are also fulfilled with lentils. From Fig.(7) we see that the model determined for the spheres in [4] behaves reasonably well for the experimental values of our ellipsoids, even though it seems to have an underestimation for the largest cylinder.

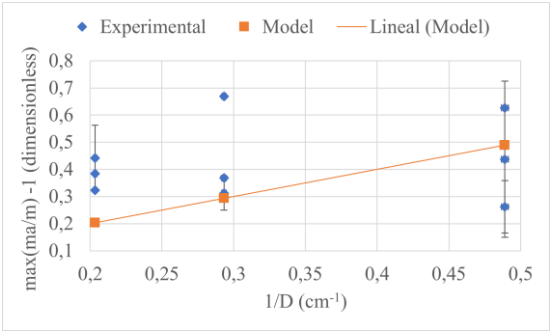

FIG.7: Comparison of the maximum deviation from the fluid behaviour between experimental values for ellipsoids and the model determined for spheres Eq.(9) versus the inverse of the diameter of the cylinder.

From the determined packing fraction, I can use Eq.(11) and the fact that $\rho=M/V$ to obtain h_a, h^* and h_d by using M, m_a, m^* and m_d respectively. The results are shown in Fig.(8).

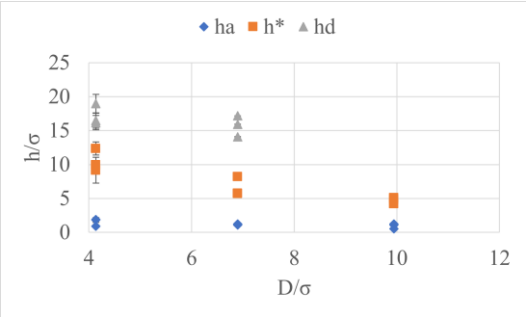

FIG.8: Comparison of the characteristic heights obtained in the experiments normalized by the mean diameter versus the normalized diameter of the cylinder.

By comparing the results in [4] with Fig.(8) it can be seen that the behaviour in both cases is similar and that the characteristic heights do not vary much between experiments with the same cylinder. This heights tend to decrease as we increase the diameter of the container. Note that I have not determined the value of f for the small cylinder since the results obtained were not mathematically possible, probably due to parallax errors in the photos captured with the camera from which we determine the column height. However, the characteristic heights that are represented in Fig.(8) for this cylinder are computed by measuring directly the height in *MatLab* and shall be taken as an estimation. The values for the other packing fractions are consistent with the results in [8], considering that our mean aspect ratio is $\alpha = 0.49$.

IV. CONCLUSIONS

- The main factor for the reverse Janssen effect is the ratio D/σ, since a change in the grain geometry does not make this phenomenon to disappear.
- Packing fractions seem to play a role in where the overshoot starts, as more packed grains such as the ellipsoids deviate from the fluid with less added mass than in the case of spheres.
- The maximum deviation between apparent and added mass can be considered proportional to $1/D$ as in the case of spheres. However, these results should be complemented with more experiments to have better statistics.

Acknowledgments

I would like to thank Alberto and Ramon for giving me the opportunity to work as a physicist in this project. I also want to thank the group for all the work that lead to these experiments and for helping me when needed, specially to Bernat, Jyo and Caleb. Finally, I want to thank my family and friends for their support during all this tough year.

[1] H. A. Janssen, *Z. Verein Deutsch. Ing.* vol. 39, pp. 1045, 1895.

[2] M. Sperl «Experiments on Corn Pressure in Silo Cells – Translation and Comment of Janssen's Paper from 1895», *Ganular Matter*, vol. 8, pp. 59-65, 2008.

[3] A. Qadir, et al. «Validity of the Janssen Model for Layered Structures in a Silo», *Mehran University research journal of Engineering and Technology*, vol. 30, pp. 405-410, 2011.

[4] S. Mahajan et al, «Reverse Janssen Effect in Narrow Granular Columns», *Phys. Rev. Lett.*, vol. 124, 128002, 2020.

[5] J. H. Shaxby and J. C. Evans, *Trans. Faraday Soc.*, vol 19, pp. 60, 1923.

[6] F.A.L. Dullien, Porous Media: Fluid Transport and Pore Structure, New York: Academic Press, 1992.

[7] H. Solomon, «Random Packing Density» Technical report no. 105, University of Stanford, Department of Statistics, 1965.

[8] F. Schaller, «The Structure of Random Ellipsoid Packings.» PhD diss., Universität Erlanger-Nürnberg, 2012.